


# DNA Loading and Release Using Custom-Tailored Poly(L-lysine) Surfaces

Amin Shakiba,<sup>†</sup> Sagar L. Patil,<sup>‡</sup> Oussama Zenasni,<sup>†</sup> Monika E. Schmitt,<sup>†</sup> Preethi H. Gunaratne,<sup>‡</sup> and T. Randall Lee<sup>\*,†</sup> 

<sup>†</sup>Departments of Chemistry and Chemical Engineering and the Texas Center for Superconductivity, University of Houston, Houston, Texas 77204-5003, United States

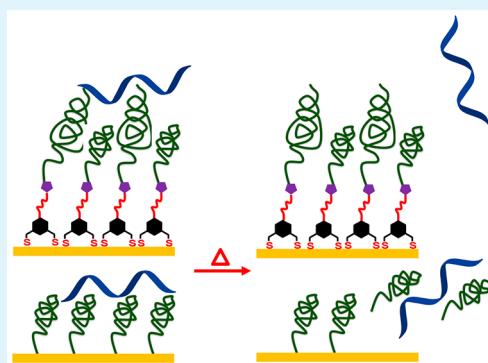
<sup>‡</sup>Department of Biology and Biochemistry, University of Houston, Houston, Texas 77204-5001, United States

## Supporting Information

**ABSTRACT:** This Article describes the generation and study of surfaces modified with custom-crafted poly(L-lysine) (PLL) coatings for use in the loading and delivery of single-stranded DNA (ssDNA). The experimental strategy utilizes bidentate dithiol adsorbates to generate stably bound azide-terminated self-assembled monolayers (SAMs) on gold possessing an oligo(ethylene glycol) (OEG) spacer. Consequent to the molecular assembly on gold, the azide termini are covalently attached to a maleimide linker moiety via a copper-catalyzed azide–alkyne “click” reaction. Functionalization with maleimide provides a platform for the subsequent attachment of cysteine-terminated poly(L-lysine) (PLL), thus forming a suitable surface for the loading of ssDNA via electrostatic interactions. In efforts to maximize DNA loading, we generate SAMs containing mixtures of short and long PLL segments and explore the DNA-loading capability of the various PLL SAMs.

We then use thermal increases to trigger the release of the ssDNA from the surface. By examining the loading and release of ssDNA using these new two-dimensional systems, we gain preliminary insight into the potential efficacy of this approach when using three-dimensional gold nanostructure systems in future gene-delivery and biosensing applications.

**KEYWORDS:** self-assembled monolayers, bidentate, poly(L-lysine), DNA, loading, release



## INTRODUCTION

Continuing reports describe the growing uses of gold nanoparticles to engineer drug carriers.<sup>1–3</sup> Oligonucleotides such as small interfering RNAs (siRNAs) are important therapeutic agents in such diseases as cancer, autoimmune disorders, dominant genetic disorders, and viral infections.<sup>4</sup> Delivered intracellularly, siRNAs bind and degrade messenger RNAs (mRNAs) with high specificity.<sup>4</sup> Many platforms are being tested for intracellular delivery and stabilization of siRNAs.<sup>3–6</sup> However, controlling the delivery process of drugs to the targeted cells remains a daunting hurdle.<sup>7</sup> Developing a smart or “on-demand” drug vehicle capable of delivering the payload to the right place and at the right time has come to the forefront of this line of research. In such smart vehicles, coating molecules (e.g., molecular adsorbates) are widely used to stabilize the colloidal system and facilitate the process of drug delivery.<sup>8</sup> In particular, self-assembled monolayers (SAMs) in which organic adsorbates spontaneously attach to a metal surface (especially gold) have been used to tailor the interfacial properties of the carriers.<sup>9</sup> Specifically, adsorbates on a gold surface are composed of a headgroup, a spacer, and a terminal group; typically, the headgroup contains sulfur. The spacer, which separates the headgroup and the chain terminus, serves as a barrier between the metal surface and the SAM interface.

Separately, the terminal group can be used to introduce specific functionalities that govern the interactions between the coated surface and the surrounding media (e.g., for tailoring interactions with biomolecules). In fact, several research groups have used this type of SAM to design functionalized gold surfaces for drug-delivery purposes.<sup>8</sup>

In recent years, the field of drug delivery witnessed several new protocols and materials for controlled drug release. In such delivery systems, a response to an external stimulus causes an “on-demand” release of therapeutic agents.<sup>10</sup> For example, thermal energy has been used successfully as an external stimulus to trigger drug release from nanocarriers.<sup>11</sup> In addition, gold nanostructures are good candidates for such nanocarriers due to their plasmonic properties, including their ability to generate heat energy in response to optical stimulation (particularly at tissue-transparent near-infrared wavelengths).<sup>12,13</sup> Importantly, incorporating thermally responsive SAMs enhances the efficiency of the drug-release system. However, retaining the structure of the initial film after thermal treatment remains a challenge. Recent work with multidentate

**Received:** April 10, 2017

**Accepted:** June 21, 2017

**Published:** June 21, 2017



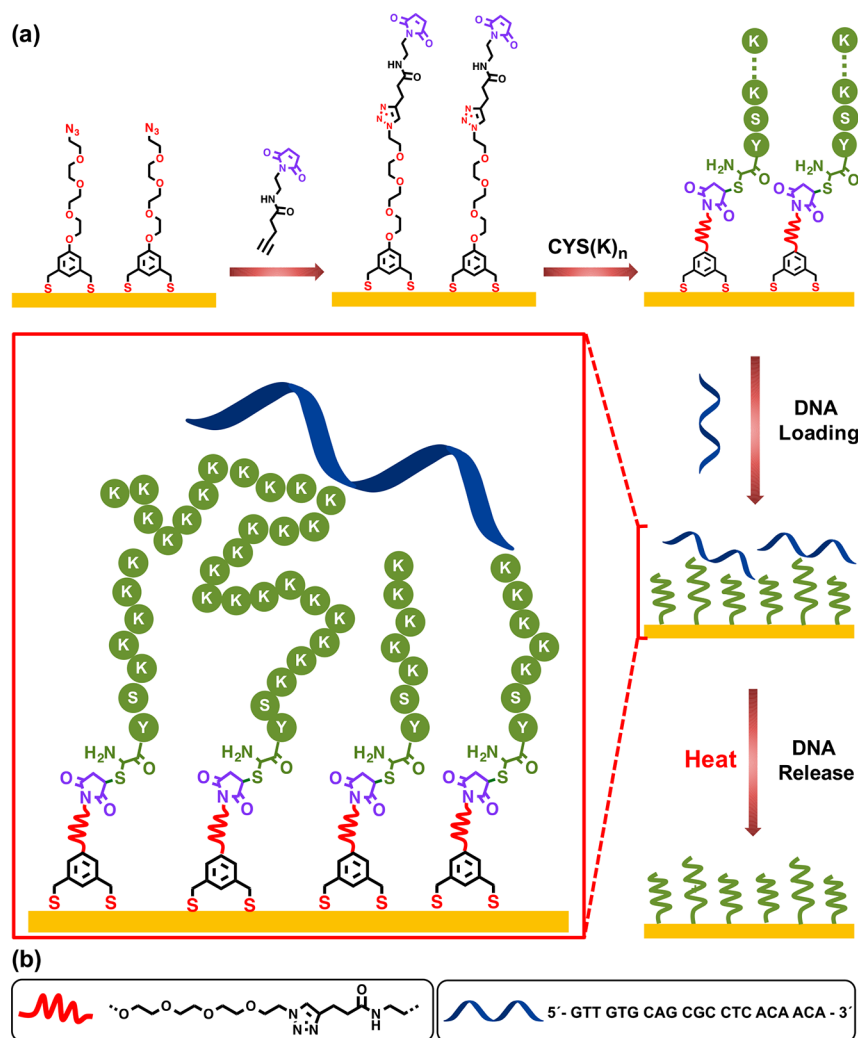


**Figure 1.** Illustration of the loading and release of ssDNA molecules from a custom-tailored PLL surface. (a) In the stepwise molecular assembly on gold, the maleimide linker moieties are covalently attached to the azido surfaces via a click reaction. Functionalization with maleimide provides a platform for the subsequent attachment of cysteine-terminated poly(L-lysine) (PLL). A mixed PLL film composed of short (8 amino acids; CYS(K)<sub>8</sub>) and long (28 amino acids; CYS(K)<sub>28</sub>) peptide chains exposes positive charges onto which ssDNA attaches electrostatically. Subsequent thermal treatment of the surface initiates the release of the ssDNA molecules. (b) The chemical structure of the spacer group and the sequence of the ssDNA.

thiols showed that these films form SAMs on gold nanoparticles that are more thermally robust than those derived from monodentate thiols.<sup>14–16</sup> As such, bidentate adsorbates can serve as a suitable partitioning layer to act as a payload carrier that can withstand thermal stress during thermally modulated payload release.

Recently, we reported the synthesis and study of a dithiol adsorbate that was designed for use as a thermally stable platform for attaching maleimide moieties onto the surface of gold.<sup>17</sup> The attachment of maleimide was followed by the attachment of cysteine-terminated poly(L-lysine) (PLL) to introduce multiple positive charges that would hypothetically facilitate the electrostatic attachment of model therapeutic oligonucleotides (e.g., ssDNA, with its negatively charged phosphate backbone) onto the surface. In our design strategy, we proposed that the subsequent introduction of thermal energy could be used to modulate the interactions between the oligonucleotides and the PLL termini, thereby releasing ssDNA molecules from the surface. The potential reversibility of this system makes it attractive for use in biomedical applications

such as biosensors, therapeutic diagnosis, and drug delivery.<sup>2,18–21</sup> In particular, the noncovalent attachment of DNA onto the PLL surfaces provides a reversible interaction that offers a loading-and-release mechanism for therapeutic oligonucleotides. Thus, this strategy offers a robust surface coating that is capable of acting as a responsive (i.e., smart) drug-release layer.

To implement this strategy in the present investigation, we synthesized a unique bidentate adsorbate (5-(2-(2-(2-(2-azidoethoxy)ethoxy)ethoxy)ethoxy)-1,3-phenylene)-dimethanethiol (N3OEGBnDT) that possesses an azide terminus and a water-soluble adhesion-resistant oligo(ethylene glycol) (OEG) linker moiety.<sup>22</sup> Using N3OEGBnDT, we generated a primary monolayer on the gold surface (see Figure 1a). Next, we used a copper(I)-catalyzed click reaction to attach a specifically designed maleimide linker to the azide-terminated SAM, thus providing a covalent binding site for cysteine-terminated PLL via Michael addition (Figure 1a).

This new functional PLL surface serves as a vehicle upon which therapeutic agents such as ssDNA can be loaded via

electrostatic interactions and released upon treatment with heat, as illustrated in Figure 1b. We used ellipsometry, polarization modulation-infrared reflection-adsorption spectroscopy (PM-IRRAS), and X-ray photoelectron spectroscopy (XPS) to characterize the formation of monolayer films and investigate the attachment of cysteine-terminated PLL onto maleimide-functionalized surfaces. We define “optimal PLL surfaces” as those capable of loading and releasing short ssDNA. This flexible and stable platform provides a reliable and efficient carrier for targeted gene-delivery applications.

## EXPERIMENTAL SECTION

A description of all materials, synthetic procedures, protocols, and analytical instruments used is provided in the Supporting Information, which also includes mass spectral data and  $^1\text{H}$  and  $^{13}\text{C}$  NMR spectra for the adsorbate (5-(2-(2-(2-(2-azidoethoxy)ethoxy)ethoxy)ethoxy)-1,3-phenylene)dimethanethiol (N3OEGBnDT; see Figures S1 and S2).

## RESULTS AND DISCUSSION

**Analysis by Ellipsometry and XPS of Maleimide-Functionalized SAMs.** On the basis of the success of our recently reported strategy to form maleimide-functionalized monolayers using dithiol adsorbates,<sup>17</sup> we prepared a new azide-terminated dithiol adsorbate (see the Supporting Information) for generating SAMs on gold that have the capacity to act as a primary attachment site for the click reaction with a maleimide linker. Specifically, we designed the adsorbate to possess an azide-terminus and an OEG linker due to (1) the specificity of the azide-based click reaction,<sup>23</sup> and (2) the good water solubility and antiadhesiveness<sup>24</sup> of the OEG group, respectively. The inherent features of OEG moieties should facilitate the use of this technology in biological media where antigen specificity and water solubility are advantageous.<sup>25</sup>

Table 1 shows the ellipsometric thicknesses of the N3OEGBnDT monolayers following the formation of azide-

**Table 1. Ellipsometric Thickness of SAMs Derived from N3OEGBnDT before and after Reaction with Maleimide Linker**

SAMs	thickness (Å)
azide-terminated	12.7 ± 0.4
maleimide-terminated	21.9 ± 0.6
1-octadecanethiol <sup>a</sup>	22.9 ± 1.1

<sup>a</sup>Data for this SAM are provided as a standard.

terminated SAMs and functionalization with maleimide via click reaction. In principle, the structural arrangement of OEG-based adsorbates should produce an incremental increase in thicknesses of 2.78 Å per EG unit ( $-\text{OCH}_2\text{CH}_2-$ ),<sup>26</sup> which translates to an expected thickness of  $\sim 16$  Å for SAMs derived from N3OEGBnDT. However, the measured thickness value presented in Table 1 is lower than the expected value by  $\sim 3$  Å. The low value is probably due in part to the increased spacing between the aromatic moieties in this type of SAM as described in a previous report,<sup>16</sup> leading to the formation of SAMs with reduced packing density as compared to SAMs derived from monodentate adsorbates. Nevertheless, the observed increase in thickness from 12.7 to 21.9 (i.e.,  $\Delta$ thickness  $\sim 9$  Å) in the subsequent step is consistent with a largely successful click

reaction: our calculations suggested an increase in thickness of  $\sim 13$  Å based on the length/structure of the maleimide linker.<sup>17</sup>

Separately, we verified the formation of azide- and maleimide-terminated surfaces using analysis by XPS, where we examined the detailed chemical composition of these surfaces by analyzing the C 1s, N 1s, and O 1s binding energy regions (Figure 2). In the C 1s region, the peaks at binding energy (BE)  $\sim 286.5$  eV indicate the presence of the ether carbons of the OEG chains,<sup>26,27</sup> whereas the peaks at  $\sim 285$  eV are characteristic of saturated hydrocarbons.<sup>17,27</sup> After attaching the maleimide linker to the surface, a new peak appears at 288–289 eV corresponding to the carbons in the C=O bonds in the maleimide termini. Additionally, the peaks for binding energies at 286–287 eV represent the carbon atoms from the C–N and C–O moieties in the SAMs, and the shoulder peak at  $\sim 285$  eV represents the attenuated C 1s core electrons of carbons in the aromatic ring and saturated hydrocarbons within and near the underlying headgroup.

The N 1s binding region also provides a tool for detecting the successful attachment of the maleimide linker (see Figure 2b). The band at  $\sim 404$  eV is associated with the core electrons from the high oxidation state nitrogen of the azide group.<sup>28</sup> This band disappears after the click reaction, which is also accompanied by a broadening of the peak at 400 eV due to core electrons from the nitrogens of the amide and triazole functional groups, which appear at  $\sim 400$  eV.<sup>28</sup>

Additional evidence supporting the presence of the OEG-dithiol adsorbates and maleimide linkers can be found in the O 1s binding region shown in Figure 2c. The peak centered at  $\sim 532.8$  eV for the N3OEGBnDT SAM corresponds to the oxygens of ethylene glycol. After the attachment of the maleimide linker, a shoulder appears at a lower BE ( $\sim 532.1$  eV), which corresponds to the oxygen in the C=O bonds of the maleimide terminal group.<sup>28,29</sup>

**Poly(L-lysine) Attachment.** As shown in previous studies,<sup>30,31</sup> peptides react with gold surfaces; consequently, an effective barrier is needed to generate functional peptide-terminated SAMs on gold. Also, the thiol-maleimide Michael addition is a reliable reaction for attaching biomolecules to a surface.<sup>32</sup> Herein, we use this strategy to attach cysteine-terminated PLL to our custom-designed bidentate-based maleimide SAMs. Analysis by XPS of the resulting surfaces allowed us to identify the optimal conditions for attaching PLL to the maleimide-functionalized surfaces.

**Formation of Mixed Poly(L-lysine) Films.** We performed our experiments in a buffer at pH = 7.4, which is a typical physiological pH used in cell studies.<sup>2,21</sup> On the basis of previous PLL studies, we likely obtained random coil structures.<sup>33,34</sup> At a pH level lower than the  $\text{pK}_a$  of poly(L-lysine) ( $\text{pK}_a = \sim 10$ –11), protonation of the amine groups disrupts the hydrogen bonding and consequently the helical structure.<sup>34,35</sup> The ellipsometric measurements show an increase of only  $\sim 15$  Å following the attachment of PLL onto the surface (see Table S1). We hypothesize that the observed small increase in thickness might be due to electrostatic repulsion between the positively charged random coil polypeptides, which prevents the closely packed alignment of the peptide chains on the surface. Nevertheless, our peptide layer is markedly thicker than that of contemporary work.<sup>36</sup> To enhance the immobilization of PLL (and subsequently ssDNA), we chose to use a mix of PLL5 and PLL25 (i.e., PLL with 5 and 25 lysine residues, respectively). Our series ranged from 100% PLL25 (i.e., mole fraction of 100% PLL25 and 0% PLL5) to

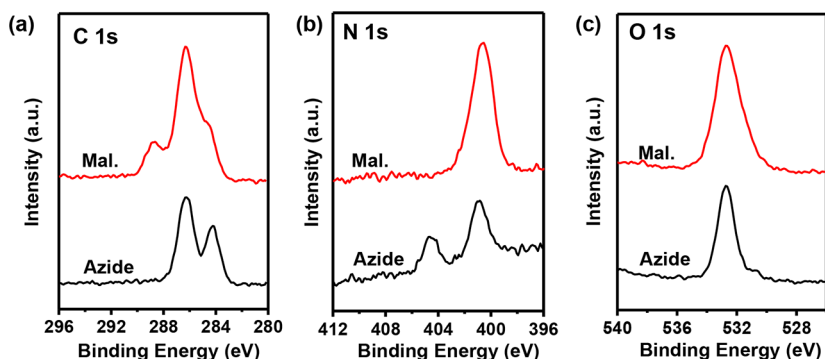


**Figure 2.** XPS spectra of azide-terminated and maleimide-terminated SAMs. (a) C 1s binding region showing peaks for the C–C and C–H BE (284–285 eV) and for C–O BEs (286–287 eV) appear for azide SAMs. After attachment of the maleimide linker, a peak appears at BE  $\sim$ 289 eV corresponding to carbons in the C=O bonds. (b) N 1s binding region showing a peak at  $\sim$ 404 eV corresponding to the nitrogen with a high oxidation state in the azide SAMs, which disappears after maleimide attachment. The initial azide peak at  $\sim$ 400 eV broadens after maleimide attachment due to the nitrogens from the amide and triazole functional groups. (c) O 1s binding region showing the appearance of a broad shoulder at 532.1 eV following maleimide attachment.

0% PLL25 (i.e., mole fraction of 0% PLL25 and 100% PLL5) in intervals of 20%.

To evaluate the attachment of mixed PLL films on gold, we used PM-IRRAS analysis, which can provide insight into film composition. As shown in Figure 3, a strong C=O stretching

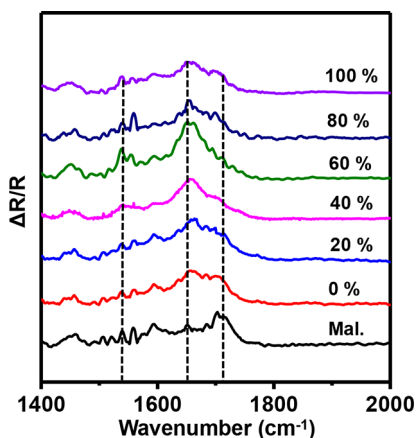


**Figure 3.** PM-IRRAS spectra of SAMs depicting pre/post attachment of a series of mixed-length cysteine-terminated PLL moieties onto maleimide-terminated surfaces as indicated by the percentage of PLL25 used in the series. The band at  $\sim$ 1710  $\text{cm}^{-1}$  corresponds to the C=O stretching of the imide bond of the maleimide group. After attachment of PLL, an amide I bond arises at  $\sim$ 1660  $\text{cm}^{-1}$ , and an amide II band appears at  $\sim$ 1540  $\text{cm}^{-1}$ .

vibration associated with the imide carbonyl of the maleimide moieties appears at  $\sim$ 1710  $\text{cm}^{-1}$ . Following the attachment of PLL, a significant peak appears at  $\sim$ 1660  $\text{cm}^{-1}$  along with a less intense peak at  $\sim$ 1540  $\text{cm}^{-1}$ , which together indicate the presence of the amide I and II bands of a polypeptide moiety. The position of the amide I and II bands demonstrates the conformation of a polypeptide. A poly(L-lysine) generally shows amide I and II peaks at  $\sim$ 1650–1670 and  $\sim$ 1540–1550  $\text{cm}^{-1}$ , respectively.<sup>34–37</sup> Analysis by PM-IRRAS therefore confirmed the attachment of PLL onto the maleimide SAMs. Additionally, Figure 3 shows PM-IRRAS spectra for the series of mixed PLL films. A comparison between the relative intensity of the amide I peak at  $\sim$ 1660  $\text{cm}^{-1}$  (an indication of PLL) to that of the imide peak (an indication of maleimide) at  $\sim$ 1710  $\text{cm}^{-1}$  indicates that PLL25 60% exhibits the most

effective attachment of PLL onto the maleimide-functionalized surfaces.

For complementary characterization of the mixed PLL monolayers, we analyzed the corresponding films by XPS. Figure 4 shows the XPS spectra of the C 1s, N 1s, and O 1s binding energy regions obtained from the mixed monolayer surfaces. In the C 1s region (Figure 4a), the peak at BE  $\sim$ 285 eV appears after the attachment of PLL. This peak represents saturated carbon atoms in an aliphatic chain, including those in the lysine moieties.<sup>38</sup> The N 1s spectra (Figure 4b) show a shoulder at 402 eV represented by a dashed line that corresponds to the nitrogens in the C–N bonds of the protonated amine of the lysine group. In the O 1s binding region (Figure 4c), a peak arises at  $\sim$ 531.8 eV after peptide attachment. This peak, represented by a dashed-line at the lower BE, corresponds to the carbons in the C=O bonds of the amide in the peptide chains.<sup>38</sup>

A qualitative assessment of the mixed PLL SAMs by XPS and PM-IRRAS suggests that, of the series tested, the most efficient attachment of polypeptide molecules to the surface is achieved by SAMs developed from PLL25 60%. Subsequently, we quantified the efficiency of PLL attachment by integrating the area under the peaks of key elements in the XPS spectra. The signal area represents the amount of each element on the surface. The increase in the area for each signal after PLL attachment reflects the increase of each element and, consequently, the amount of PLL. For each set of SAMs, we normalized the ratio of each peak in a specific binding region to that of Au 4f. Examining changes in the C 1s and N 1s signals after the attachment of the cysteine-terminated PLL to the maleimide-functionalized surfaces allowed us to compare different monolayers and to quantify in a relative sense the efficiency of the PLL attachment (see Table 2). This method is an alternative means to evaluate the efficiency of attachment of each mixed-SAM system.

As shown in Figure 4, normalized XPS data show an increase in the carbon and nitrogen signals for each mixed-SAM system; Table 2 details the significant increases in the nitrogen and carbon signals. Note that mixed-PLL SAMs with 60% PLL25 show 56% and 250% increases in C/Au and N/Au signal ratios, respectively. Thus, we conclude that the optimal ratio of 60% PLL25 to 40% PLL5 exhibits an enhanced arrangement of the



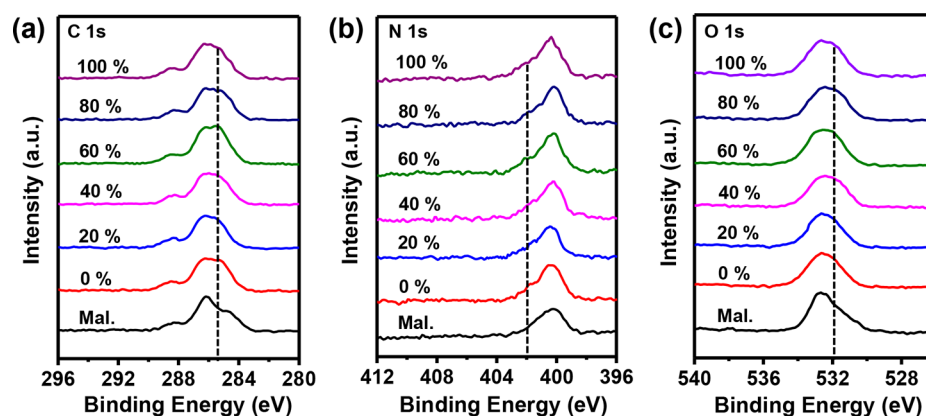


**Figure 4.** XPS spectra of SAMs depicting pre/post attachment of a series of mixed-length cysteine-terminated PLL moieties onto maleimide-terminated surfaces as indicated by the percentage of PLL25 used in the series. (a) C 1s binding energy region (284–285 eV), where the intensity of C–C and C–H peaks increases after PLL attachment. (b) N 1s binding energy region shows an increase in the shoulder at  $\sim 402$  eV after PLL attachment. (c) O 1s binding energy region shows a shoulder at 531.8 eV that increases after PLL attachment.

**Table 2.** Increase of XPS Signal after Attachment of PLL as Compared to Maleimide-Functionalized Surfaces

% PLL25 used for formation of SAMs	% increase of C/Au	% increase of N/Au
100	$29 \pm 9$	$90 \pm 5$
80	$48 \pm 11$	$241 \pm 8$
60	$56 \pm 6$	$250 \pm 13$
40	$33 \pm 3$	$148 \pm 3$
20	$26 \pm 2$	$122 \pm 8$
0	$19 \pm 6$	$87 \pm 9$

PLL chains on the SAM surface that leads to an increase in the efficiency of PLL attachment.

*Thermal Stability of SAMs Derived from Bidentate Dithiol Adsorbates.* Because the ultimate goal of designing this system is to release the payload selectively from the surface upon exposure to heat, the stability of the underlying SAMs is crucial for the success of such a system, lest the components of the SAM be delivered too. A primary SAM derived from monodentate thiols desorbs spontaneously upon increasing the temperature of the surrounding media,<sup>14,16</sup> which limits the use of monodentate thiol-based SAMs in photothermal applications. However, the use of adsorbates with bidentate headgroups leads to SAMs with substantially enhanced thermal stabilities.<sup>14,16</sup> To ensure the overall thermal stability of the carrier in the system studied here, we utilized a SAM having the

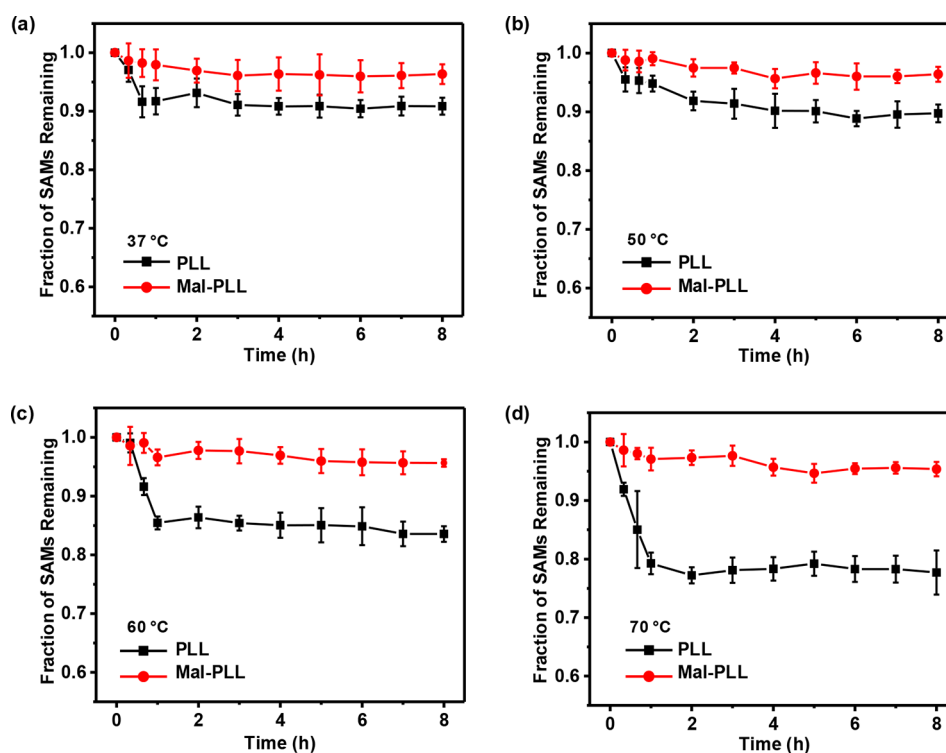


**Figure 5.** Thermal stability test of PLL5 SAMs on gold showing the desorption of the monolayers at (a) 37, (b) 50, (c) 60, and (d) 70 °C. The red lines correspond to the bidentate PLL5 SAM system derived via the maleimide linker, and the black lines correspond to SAMs generated via the direct attachment of PLL5 having an  $\omega$ -cysteine moiety.

most robust bidentate dithiol headgroup developed thus far (i.e., one having a 3,5-bis(mercaptomethyl)phenoxy headgroup).<sup>16</sup>

We examined the thermal stability of the PLLS-coated surfaces by evaluating changes in the thickness of the monolayers at variable temperatures over a selected period of time. Measurements of ellipsometric thickness were acquired in 20 min intervals for the first 2 h and in 1 h intervals thereafter. Figure 5a–d displays the changes in the thickness of the monolayers at the set temperatures of 37, 50, 60, and 70 °C in water. We also compared the thermal stability of the bidentate PLLS-functionalized surfaces to that of SAMs generated from the direct attachment of PLLS having an  $\omega$ -cysteine moiety. At all temperatures, the results indicate that the SAMs derived from the bidentate PLLS system are markedly more thermally stable (i.e., they desorb substantially less) than those derived from the direct attachment of PLLS having an  $\omega$ -cysteine moiety. Importantly, the difference is magnified at elevated temperatures, and particularly at the highest temperature examined (70 °C). When taken as a whole, these results illustrate the unique and important enhancement in stability afforded by the bidentate 3,5-bis(mercaptomethyl)phenoxy headgroup.

**DNA Loading on PLL-Functionalized Surfaces.** In the next phase of this investigation, we examined the immobilization of the negative phosphate backbone of ssDNA on the PLL surfaces via electrostatic interactions. When compared to a simple surface-bound model, we hypothesized that intercalation of ssDNA into the PLL layer might lead to enhanced loading. As a starting point in evaluating the DNA loading capacity of our system, we initially evaluated SAMs generated via the direct attachment of PLL having an  $\omega$ -cysteine moiety. The ellipsometric thickness and XPS measurements indicated insufficient loading of ssDNA on these surfaces (see Table S2); notably, XPS has been used to assess quantitatively the binding of ssDNA on SAMs.<sup>39</sup> One rationalization for the poor loading on these SAMs is that thin films of pure PLL likely generate relatively rigid and/or uniform monolayers where ssDNA species lay on top of the surface, thus leading to minimal charge–charge interactions between the PLL moieties and ssDNA and thus poor loading. Moreover, the direct attachment of PLL lacks the aforementioned advantages of using a bidentate adsorbate platform. In efforts to achieve a more efficient system, we examined DNA loading on a series of mixed-PLL SAMs assembled on the custom-tailored bidentate adsorbate layer where the length of the PLL chain was varied (i.e., PLL5 plus PLL25). Following DNA loading, it is unclear what 3D structure might be triggered, although a report proposed that the rapid interaction of PLL and ssDNA leads to a stable structure between PLL-DNA due to the electrostatic interactions between the two moieties, as well as their hydrogen bonds.<sup>40</sup> In this series, we hypothesized that ssDNA would be able to penetrate into the PLL layer, leading to an increase in the number of charge–charge interactions and higher loading.

**Loading of ssDNA on Mixed Poly(L-lysine) SAMs.** To maximize ssDNA loading, we assessed a series of mixed PLL films comprised of SAMs derived from PLL5 and PLL25. Using ellipsometry, we evaluated the increase in thickness after ssDNA immobilization. Previous studies suggested that ssDNA tends to adopt a “lying-down” conformation on charged surfaces.<sup>41–43</sup> As shown in Table 3, analysis by ellipsometry of the surfaces examined here supports the hypothesis that ssDNA adopted a lying-down conformation. The one exception is the

**Table 3. DNA Loading Analysis: Increased Thickness and P/Au XPS Signal Ratio after Loading of the ssDNA**

% PLL25 used for formation of SAMs	$\Delta T$ (Å)	P/Au
100	4.2 ± 0.3	0.0057 ± 0.0005
80	4.2 ± 0.7	0.0056 ± 0.0002
60	5.3 ± 0.4	0.0061 ± 0.0003
40	7.3 ± 0.2	0.0072 ± 0.0006
20	4.2 ± 0.7	0.0055 ± 0.0002
0	2.8 ± 0.9	0.0027 ± 0.0004

SAM developed from 40% PLL25 (i.e., the mixed SAM formed from a solution containing 40% PLL25 and 60% PLL5). This particular mixed PLL SAM shows the largest increase in thickness following ssDNA loading, which suggests enhanced incorporation of ssDNA into the PLL film. Separately, analysis by XPS of these films (vide infra) demonstrates the appearance of a peak for phosphorus, which is consistent with the adsorption of ssDNA on the surface. For a better understanding, we integrated the area under the P 2p peaks to provide a quantitative assessment of ssDNA immobilization on the surfaces. As is indicated in Table 3, SAMs derived from 40% PLL25 show the greatest P/Au ratio, which indicates the greatest amount of ssDNA loading for this SAM system.

We also used the C/Au and N/Au signal ratios to compare the ssDNA loading on these mixed PLL SAMs (see Figure 6).

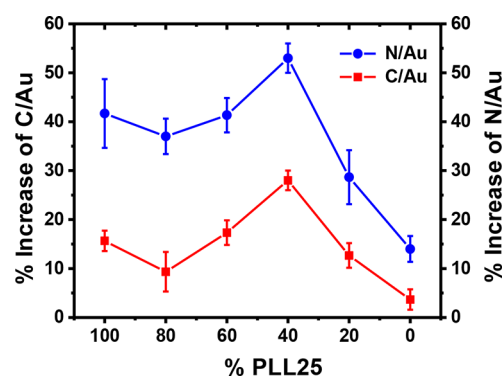


**Figure 6.** Quantitative XPS signal analysis of the percent increase of N/Au (blue ●) and C/Au (red ■) of the various PLL SAMs after exposure to ssDNA.

The comparative increase in the value of these XPS ratios reflects the relative binding affinity of ssDNA on each surface. Analysis of both the C/Au and the N/Au signal ratios shows a maximum loading capacity for the 40% PLL25 SAMs. Collectively, these results lead us to conclude that the 40% PLL25 SAMs provide the most suitable PLL chain packing density (i.e., distance between lysine chains) for ssDNA to intercalate into the film. Consequently, this particular mixed SAM system offers the maximal loading of model oligonucleotides on these PLL surfaces.

**Release of ssDNA via Heat Treatment.** We heated the samples in TE buffer solution (10 mM Tris-HCl, 1 mM EDTA; pH = 7.4) to initiate the release of short ssDNA molecules from the 40% PLL25 SAM surfaces. One previous report described the partial release of short ssDNA at temperatures as low as 30 °C.<sup>2</sup> The observation of release under these mild conditions was perhaps due to the instability of the primary adsorbate, where both the adsorbate and the payload were plausibly released. According to thermal stability results presented above,

our bidentate platform is highly stable, even at elevated temperatures. As a consequence, we expect the release of our payload without degradation of the platform. To study the release of model oligonucleotides, we heated a ssDNA-loaded substrate at 45 °C (i.e., slightly above the temperature of the human body) and monitored the ellipsometric thickness. We note that short strands of ssDNA (e.g., 18–21 base pairs) with thermal properties similar to ours (i.e., melting temperature ( $T_m$ ) of 61.1 °C; see the Supporting Information) released at temperatures as high as 70 °C or even 95 °C remain intact and expressible.<sup>2,44,45</sup> Thus, it is reasonable to conclude that the ssDNA moieties released under the mild conditions used here are robust and fully expressible. Moreover, we elected to explore our release method at a relatively low temperature as we look forward to minimizing tissue damage in clinical applications. The thickness profiles in Figure 7 illustrate a

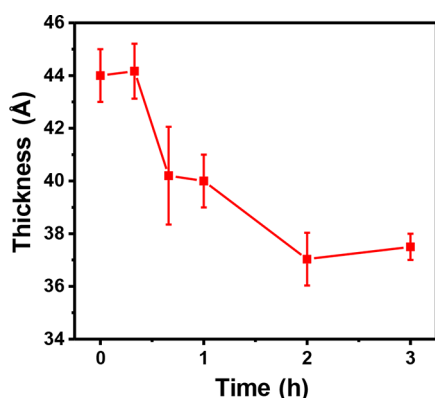


**Figure 7.** Ellipsometric thickness of ssDNA-loaded 40% PLL25 SAMs as a function of heating at 45 °C in TE buffer solution.

decrease in thickness consistent with the release of ssDNA from the 40% PLL25 SAMs. We continued to heat the samples at 45 °C for 3 h until no change in thickness was observed. Notably, the thickness of these films (~37–38 Å) is comparable to that of the pristine 40% PLL25 SAMs (~36 Å; Table S1), which is consistent with a model where no release of the bidentate platform occurs.

We confirmed the complete release of the ssDNA from the platform by evaluating the P 2p binding region by XPS. As shown in Figure 8, the disappearance of the phosphorus peak after the heating process indicated the successful release of all DNA molecules at 45 °C. Furthermore, we precluded any need for testing at higher temperatures given our observation of the complete release of ssDNA at 45 °C.

## CONCLUSIONS

We synthesized a new bidentate dithiol adsorbate for the generation of stable azide-terminated SAMs on gold possessing an oligo(ethylene glycol) (OEG) spacer to serve as an initial platform for the attachment of maleimide functional groups. Characterization of these films using ellipsometry and XPS indicated that this SAM system provided a means for the covalent attachment of PLL chains to the surface. The subsequent positively charged surface was then used to immobilize ssDNA on the surface electrostatically. This strategy is suitable for designing smart coatings for nanoparticles with the ability to bind and release DNAs or RNAs. Qualitative and quantitative analyses of the films collected by ellipsometry, PM-IRRAS, and XPS show that using a mixed ratio of PLL

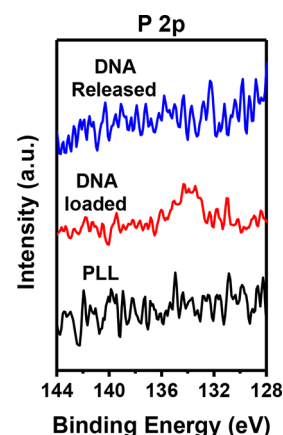


**Figure 8.** XPS spectra of the P 2p region for the 40% PLL25 SAMs before loading, after loading, and after release of ssDNA. The peak at ~133 eV appears after loading the ssDNA and corresponds to the phosphate backbone in DNA. After heating in TE buffer solution, the peak disappears, confirming the complete release of ssDNA from the surface.

molecules of different chain lengths led to maximum attachment of PLL to the surface. Additionally, studies of DNA loading showed that mixed-SAMs with 40% PLL25 provided the optimal platform for loading ssDNA. Our studies also demonstrated the successful release of ssDNA upon exposure to heat in TE buffer solution. As a whole, we introduced a custom-designed thermally stable PLL surface that has the capacity to load and release short ssDNA without loss of the primary SAM coating layer. Importantly, our mixed-PLL system showed an enhanced release efficiency of ssDNA at 45 °C as compared to a previously reported strategy.<sup>2</sup> The strategy presented here holds promise for gene-delivery applications, particularly when adapted for use with three-dimensional nanoparticle-based substrates.

## ASSOCIATED CONTENT

### Supporting Information

The Supporting Information is available free of charge on the ACS Publications website at DOI: 10.1021/acsami.7b05024.

Detailed synthetic procedures of the dithiol adsorbate and maleimide linker along with mass spectral data and <sup>1</sup>H and <sup>13</sup>C NMR spectra (Figures S1 and S2) for N3OEGBnDT; and additional analyses by ellipsometry and XPS (Tables S1 and S2) (PDF)

## AUTHOR INFORMATION

### Corresponding Author

\*E-mail: trlee@uh.edu.

### ORCID

T. Randall Lee: 0000-0001-9584-8861

### Notes

The authors declare no competing financial interest.

## ACKNOWLEDGMENTS

We thank the National Science Foundation (CHE-1411265), the Robert A. Welch Foundation (E-1320), and the Texas Center for Superconductivity for supporting this research.



## REFERENCES

- (1) Giljohann, D. A.; Seferos, D. S.; Daniel, W. L.; Massich, M. D.; Patel, P. C.; Mirkin, C. A. Gold Nanoparticles for Biology and Medicine. *Angew. Chem., Int. Ed.* **2010**, *49*, 3280–3294.
- (2) Huschka, R.; Barhoumi, A.; Liu, Q.; Roth, J. A.; Ji, L.; Halas, N. J. Gene Silencing by Gold Nanoshell-Mediated Delivery and Laser-Triggered Release of Antisense Oligonucleotide and siRNA. *ACS Nano* **2012**, *6*, 7681–7691.
- (3) Ghosh, R.; Singh, L. C.; Shohet, J. M.; Gunaratne, P. H. A Gold Nanoparticle Platform for the Delivery of Functional MicroRNAs Into Cancer Cells. *Biomaterials* **2013**, *34*, 807–816.
- (4) Aagaard, L.; Rossi, J. J. RNAi Therapeutics: Principles, Prospects and Challenges. *Adv. Drug Delivery Rev.* **2007**, *59*, 75–86.
- (5) Williford, J.-M.; Wu, J.; Ren, Y.; Archang, M. M.; Leong, K. W.; Mao, H.-Q. Recent Advances in Nanoparticle-Mediated siRNA Delivery. *Annu. Rev. Biomed. Eng.* **2014**, *16*, 347–370.
- (6) Mack, G. S. MicroRNA Gets Down to Business. *Nat. Biotechnol.* **2007**, *25*, 631–638.
- (7) Patel, P. C.; Giljohann, D. A.; Seferos, D. S.; Mirkin, C. A. Peptide Antisense Nanoparticles. *Proc. Natl. Acad. Sci. U. S. A.* **2008**, *105*, 17222–17226.
- (8) Shakiba, A.; Zenasni, O.; Marquez, M. D.; Lee, T. R. Advanced Drug Delivery via Self-Assembled Monolayer-Coated Nanoparticles. *AIMS Bioeng.* **2017**, *4*, 275–299.
- (9) Bowers, C. M.; Liao, K.-C.; Zaba, T.; Rappoport, D.; Baghbanzadeh, M.; Breiten, B.; Krzykawska, A.; Cyganik, P.; Whitesides, G. M. Characterizing the Metal–SAM Interface in Tunneling Junctions. *ACS Nano* **2015**, *9*, 1471–1477.
- (10) Yang, H.; Yuan, B.; Zhang, X.; Scherman, O. A. Supramolecular Chemistry at Interfaces: Host–Guest Interactions for Fabricating Multifunctional Biointerfaces. *Acc. Chem. Res.* **2014**, *47*, 2106–2115.
- (11) Barhoumi, A.; Huschka, R.; Bardhan, R.; Knight, M. W.; Halas, N. J. Light-Induced Release of DNA from Plasmon-Resonant Nanoparticles: Towards Light-Controlled Gene Therapy. *Chem. Phys. Lett.* **2009**, *482*, 171–179.
- (12) Yang, X.; Yang, M.; Pang, B.; Vara, M.; Xia, Y. Gold Nanomaterials at Work in Biomedicine. *Chem. Rev.* **2015**, *115*, 10410–10488.
- (13) Abadeer, N. S.; Murphy, C. J. Recent Progress in Cancer Thermal Therapy Using Gold Nanoparticles. *J. Phys. Chem. C* **2016**, *120*, 4691–4716.
- (14) Srisombat, L.; Jamison, A. C.; Lee, T. R. Stability: A Key Issue for Self-Assembled Monolayers on Gold as Thin-Film Coatings and Nanoparticle Protectants. *Colloids Surf., A* **2011**, *390*, 1–19.
- (15) Srisombat, L.-o.; Zhang, S.; Lee, T. R. Thermal Stability of Mono-, Bis-, and Tris-Chelating Alkanethiol Films Assembled on Gold Nanoparticles and Evaporated “Flat” Gold. *Langmuir* **2010**, *26*, 41–46.
- (16) Lee, H. J.; Jamison, A. C.; Yuan, Y.; Li, C.-H.; Rittikulsittichai, S.; Ruskova, I.; Lee, T. R. Robust Carboxylic Acid-Terminated Organic Thin Films and Nanoparticle Protectants Generated from Bidentate Alkanethiols. *Langmuir* **2013**, *29*, 10432–10439.
- (17) Shakiba, A.; Jamison, A. C.; Lee, T. R. Poly(L-lysine) Interfaces via Dual Click Reactions on Surface-Bound Custom-Designed Dithiol Adsorbates. *Langmuir* **2015**, *31*, 6154–6163.
- (18) Zheng, Y.; Lalander, C. H.; Thai, T.; Dhuey, S.; Cabrini, S.; Bach, U. Gutenberg-Style Printing of Self-Assembled Nanoparticle Arrays: Electrostatic Nanoparticle Immobilization and DNA-Mediated Transfer. *Angew. Chem., Int. Ed.* **2011**, *50*, 4398–4402.
- (19) Moratz, J.; Samanta, A.; Voskuhl, J.; Mohan Nalluri, S. K.; Ravoo, B. J. Light-Triggered Capture and Release of DNA and Proteins by Host–Guest Binding and Electrostatic Interaction. *Chem. - Eur. J.* **2015**, *21*, 3271–3277.
- (20) Tjong, V.; Tang, L.; Zauscher, S.; Chilkoti, A. “Smart” DNA Interfaces. *Chem. Soc. Rev.* **2014**, *43*, 1612–1626.
- (21) Stobiecka, M.; Hepel, M. Double-Shell Gold Nanoparticle-Based DNA-Carriers with Poly-L-lysine Binding Surface. *Biomaterials* **2011**, *32*, 3312–3321.
- (22) von Maltzahn, G.; Ren, Y.; Park, J.-H.; Min, D.-H.; Kotamraju, V. R.; Jayakumar, J.; Fogal, V.; Sailor, M. J.; Ruoslahti, E.; Bhatia, S. N. In Vivo Tumor Cell Targeting with “Click” Nanoparticles. *Bioconjugate Chem.* **2008**, *19*, 1570–1578.
- (23) Su, J.; Mrksich, M. Using Mass Spectrometry to Characterize Self-Assembled Monolayers Presenting Peptides, Proteins, and Carbohydrates. *Angew. Chem., Int. Ed.* **2002**, *41*, 4715–4718.
- (24) Zorn, S.; Skoda, M. W. A.; Gerlach, A.; Jacobs, R. M. J.; Schreiber, F. On the Stability of Oligo(ethylene glycol) (C<sub>11</sub>EG<sub>6</sub>OMe) SAMs on Gold: Behavior at Elevated Temperature in Contact with Water. *Langmuir* **2011**, *27*, 2237–2243.
- (25) Dai, Q.; Walkey, C.; Chan, W. C. W. Polyethylene Glycol Backfilling Mitigates the Negative Impact of the Protein Corona on Nanoparticle Cell Targeting. *Angew. Chem., Int. Ed.* **2014**, *53*, 5093–5096.
- (26) Harder, P.; Grunze, M.; Dahint, R.; Whitesides, G. M.; Laibinis, P. E. Molecular Conformation in Oligo(ethylene glycol)-Terminated Self-Assembled Monolayers on Gold and Silver Surfaces Determines Their Ability To Resist Protein Adsorption. *J. Phys. Chem. B* **1998**, *102*, 426–436.
- (27) Lee, H. J.; Jamison, A. C.; Lee, T. R. Two Are Better than One: Bidentate Adsorbates Offer Precise Control of Interfacial Composition and Properties. *Chem. Mater.* **2016**, *28*, 5356–5364.
- (28) Collman, J. P.; Devaraj, N. K.; Eberspacher, T. P. A.; Chidsey, C. E. D. Mixed Azide-Terminated Monolayers: A Platform for Modifying Electrode Surfaces. *Langmuir* **2006**, *22*, 2457–2464.
- (29) Lim, C. Y.; Owens, N. A.; Wampler, R. D.; Ying, Y.; Granger, J. H.; Porter, M. D.; Takahashi, M.; Shimazu, K. Succinimidyl Ester Surface Chemistry: Implications of the Competition between Aminolysis and Hydrolysis on Covalent Protein Immobilization. *Langmuir* **2014**, *30*, 12868–12878.
- (30) Gitelman, A.; Rapaport, H. Bifunctional Designed Peptides Induce Mineralization and Binding to TiO<sub>2</sub>. *Langmuir* **2014**, *30*, 4716–4724.
- (31) Wetterö, J.; Hellerstedt, T.; Nygren, P.; Broo, K.; Aili, D.; Liedberg, B.; Magnusson, K.-E. Immobilized Chemoattractant Peptides Mediate Adhesion and Distinct Calcium-Dependent Cell Signaling in Human Neutrophils. *Langmuir* **2008**, *24*, 6803–6811.
- (32) Fontaine, S. D.; Reid, R.; Robinson, L.; Ashley, G. W.; Santi, D. V. Long-Term Stabilization of Maleimide–Thiol Conjugates. *Bioconjugate Chem.* **2015**, *26*, 145–152.
- (33) Myer, Y. P. The pH-Induced Helix-Coil Transition of Poly-L-lysine and Poly-L-glutamic Acid and the 238- $\mu$ m Dichroic Band. *Macromolecules* **1969**, *2*, 624–628.
- (34) Wang, Y.; Ying Chih Chang, Y. C. Synthesis and Conformational Transition of Surface-Tethered Polypeptide: Poly(L-lysine). *Macromolecules* **2003**, *36*, 6511–6518.
- (35) Guo, Y.; Xia, F.; Xu, L.; Li, J.; Yang, W.; Jiang, L. Switchable Wettability on Cooperative Dual-Responsive Poly-L-lysine Surface. *Langmuir* **2010**, *26*, 1024–1028.
- (36) Jordon, C. E.; Frey, B. L.; Kornguth, S.; Corn, R. M. Characterization of Poly-L-Lysine Adsorption onto Alkanethiol-Modified Gold Surfaces with Polarization-Modulation Fourier Transform Infrared Spectroscopy and Surface Plasmon Resonance Measurements. *Langmuir* **1994**, *10*, 3642–3648.
- (37) Yang, C. T.; Wang, Y. L.; Yu, S.; Chang, Y. C. I. Controlled Molecular Organization of Surface Macromolecular Assemblies Based on Stimuli-Responsive Polypeptide Brushes. *Biomacromolecules* **2009**, *10*, 58–65.
- (38) Kenausis, G. L.; Vörös, J.; Elbert, D. L.; Huang, N.; Hofer, R.; Ruiz-Taylor, L.; Textor, M.; Hubbell, J. A.; Spencer, N. D. Poly(L-lysine)-g-Poly(ethylene glycol) Layers on Metal Oxide Surfaces: Attachment Mechanism and Effects of Polymer Architecture on Resistance to Protein Adsorption. *J. Phys. Chem. B* **2000**, *104*, 3298–3309.
- (39) Lane, S. M.; Monot, J.; Petit, M.; Bujoli, B.; Talham, D. R. XPS Investigation of DNA Binding to Zirconium-Phosphonate Surfaces. *Colloids Surf., B* **2007**, *58*, 34–38.



(40) Ozer, B. H.; Smarsly, B.; Antonietti, M.; Faul, C. F. J. DNA-Analogous Structures from Deoxynucleophosphates and Polylysine by Ionic Self-Assembly. *Soft Matter* **2006**, *2*, 329–336.

(41) He, L.; Langlet, M.; Stambouli, V. Role of the External NH<sub>2</sub> Linker on the Conformation of Surface Immobilized Single Strand DNA Probes and Their SERS Detection. *Appl. Surf. Sci.* **2017**, *399*, 702–710.

(42) Sukumaran, P.; Thazhe Veetil, V.; Rajappa, S.; Li, C.-Z.; Alwarappan, S. Ionic Liquid Modified N-doped Graphene as a Potential Platform for the Electrochemical Discrimination of DNA Sequences. *Sens. Actuators, B* **2017**, *247*, 556–563.

(43) Stobiecka, M.; Dworakowska, B.; Jakiela, S.; Lukasiak, A.; Chalupa, A.; Zembrzycki, K. Sensing of Survivin Mrna in Malignant Astrocytes Using Graphene Oxide Nanocarrier-Supported Oligonucleotide Molecular Beacons. *Sens. Actuators, B* **2016**, *235*, 136–145.

(44) Diaz, J. A.; Gibbs-Davis, J. M. Sharpening the Thermal Release of DNA from Nanoparticles: Towards a Sequential Release Strategy. *Small* **2013**, *9*, 2862–2871.

(45) Karni, M.; Zidon, D.; Polak, P.; Zalevsky, Z.; Shefi, O. Thermal Degradation of DNA. *DNA Cell Biol.* **2013**, *32*, 298–301.